The Saudi Dental Journal 36 (2024) 1326–1332

Contents lists available at ScienceDirect

The Saudi Dental Journal

journal homepage: www.ksu.edu.sa
www.sciencedirect.com

Original Article

The impact of hyaluronic acid coating on polyether ether ketone dental implant surface: An in vitro analysis

Mohammed Aso Abdulghafor *, Zanyar Mustafa Amin

Oral and Maxillofacial Surgery Department, College of Dentistry, University of Sulaimani, Sulaimani, Kurdistan, Iraq

ARTICLE INFO

Keywords:
Dental implant
Surface coating
Hyaluronic acid
PEEK
Osseointegration

ABSTRACT

Objective: Polyether ether ketone (PEEK), a biocompatible polymer, is being explored as an alternative to metallic alloys for dental implants due to its aesthetic and mechanical properties. This study aimed to enhance the surface biofunctionality through evaluating human MG-63 osteoblastic cell survival, proliferation, differentiation, and mineralization.

Method: Following the sandblasting and plasma treatment of the 3D-printed PEEK discs, a layer of hyaluronic acid (Hya) was coated onto the PEEK surface. Osteoblast cells were seeded onto the discs. The groups consisted of Hya-coated PEEK, uncoated PEEK, and a control group. Cell viability, proliferation, differentiation, and mineralization potential were examined after seven and twenty-one days of cell seeding using the MTT test, DAPI staining technique, alkaline phosphatase activity (ALP), and alizarin red staining.

Results: Hya-coated PEEK increased cell viability (1.48 ± 0.13, 1.49 ± 0.09) compared to the uncoated group (1.19 ± 0.06, 1.26 ± 0.07) and control group (0.98 ± 0.04, 1.00 ± 0.07) after 7 and 21 days. Proliferation rates of coated group (60.50 ± 3.08) were greater than the uncoated (50.33 ± 2.58) and control group (38.33 ± 4.88) at 21 days, respectively. Additionally, the ALP activity on Hya-coated PEEK disks (5.55 ± 0.65, 7.54 ± 0.64) was notably higher than that of the uncoated group (1.08 ± 0.49, 2.59 ± 0.68), and control group (0.16 ± 0.09, 0.34 ± 0.18) at both time periods. Alizarin red staining in the Hya-coated PEEK group (1.81 ± 0.23, 1.97 ± 0.20) was significantly greater in comparison with uncoated group (1.12 ± 0.17, 1.14 ± 0.19) and control group (0.99 ± 0.10, 0.98 ± 0.05) at both time intervals.

Conclusion: Hya's surface coating has enhanced the biofunctional properties of PEEK implant material, as demonstrated by improved cell survival, proliferation, differentiation, and mineralization potential.

1. Introduction

Over the past several decades, implant dentistry has improved oral rehabilitation for partial and total edentulism (George et al., 2023; Ismail and Hasan, 2021; Mahmood and Mahmood, 2023; Yokoi et al., 2023). Implant dentistry faces challenges in finding materials that mimic human bone physiology, because dental implants transmit external forces and are susceptible to fatigue failure. Effective implant biomaterials must exhibit fracture resistance and elasticity (Zheng et al., 2022).

The biocompatibility, mechanical characteristics, and osseointegration potential of titanium and its alloys make them ideal dental implant biomaterials (Rupp et al., 2018). Allergic responses, implant flexibility that is inconsistent with bone density, stress-shielding, cellular sensitization, an unappealing gray appearance, and radiography artifact production are problems. These challenges emphasize the necessity for a thorough evaluation and investigation of these material (Ananth et al., 2015; Bosshardt, 2017). (Ananth et al., 2015; Bosshardt et al., 2017).

In cardiovascular, orthopedic, and dental devices, biocompatible polymers and polymer-based composite materials are being employed as metallic alloy substitutes (Krishnakumar and Senthilvelan, 2021; Li et al., 2021). Polyether ether ketone (PEEK) is a commonly used substitute because of its biocompatibility, bioresistance, and aesthetic appeal (Sacks et al., 2024). With mechanical qualities comparable to those of human bone, this material has been used in traumatology, orthopedics, and spinal implants to reduce bone resorption and stress shielding (Ananth et al., 2015; Chen et al., 2023).

A successful dental implant procedure involves osseointegration, a multi-step process involving blood clot formation, mesenchymal tissue emergence, bone production, and lamellar bone formation following

* Corresponding author.
E-mail address: mohammed.abdulghafor@univsul.edu.iq (M. Aso Abdulghafor).

https://doi.org/10.1016/j.sdentj.2024.07.012
Received 29 April 2024; Received in revised form 13 July 2024; Accepted 16 July 2024
Available online 16 July 2024

implant insertion (Amengual-Peñafiel et al., 2021; Chatzopoulos and Wolff, 2023). Initiation of osseointegration requires the adsorption of plasma protein onto a hydrophilic surface. However, the bioinert and hydrophobic surface of PEEK inhibits osteoblast adhesion, differentiation, and proliferation. Fibro-integration creates a fibrous capsule around the implant instead of bone. This impairs implant-bone interaction, causing failure and indicating the material is unsuitable (Reddy et al., 2023; Ślusarczyk et al., 2024). Artificial implants must be biocompatible and bioactive to prevent allergic reactions, chemical integration, bone-like apatite layer development, and infections from infiltrating surrounding tissues (Abdulghafor et al., 2024; Kannan et al., 2024) Surface characteristics and biological components including proteins, ions, and cells affect implant bone regeneration (Wang et al., 2023).

Bioactive coatings, including osteoconductive, biocompatible, antimicrobial, sustained antibiotic release, and corrosion-resistant coatings, are promising for optimizing the surface properties of implant materials (Zhou et al., 2023). Hyaluronic acid (Hya), an extracellular matrix glycosaminoglycan, is being tested for implant use owing to its osteoconductivity, good interactions with bone progenitor cells, and secondary stability. (Luo et al., 2023). The purpose of this study was to demonstrate the surface biofunctionality of Hya-coated PEEK by analyzing the survival, proliferation, differentiation, and mineralization of human MG-63 osteoblastic cells.

2. Materials and methods

2.1. Sample selection and preparations

Using a 3D printer (Essentium HS 240 T, College Station, Texas, USA),10 mm diameter, 1 mm thick disks were made of PEEK (Victrex Manufacturing Ltd., Lancashire, United Kingdom). The print settings were 10 mm/s, 420 °C, 0.4 mm, and 0.2 mm for velocity, orifice diameter, and layer thickness, respectively.

Subsequently, the PEEK disks were sandblasted 10 mm perpendicular to the surface with 50 μm aluminum oxide particulate at 2.7 atm pressure for 15 s. Distilled water was used to ultrasonically sanitize the disks for 15 min to eliminate any remaining particles. The plasma surface treatment of PEEK disks was carried out using low-pressure pure oxygen plasma at 70C°, 0.4 mbar pressure, and 200 W' power for ten minutes.

Hya solution was prepared by dissolving 1 mg of Hya sodium salt (M_w = ~340 kDa from Streptococcus equi, Bloomage Freda Biopharm Co. Ltd., Shandong, China) in 1 mL of double-distilled water and 2.5 mg/mL 1-ethyl-3-(3-dimethylaminopropyl) carbodiimide (EDC) and 0.63 mg/mL N-hydroxysuccinimide (NHL) (Sigma Aldrich) were then added. A PEEK disks was immersed in the solution for 6 h and allowed to dry at ambient temperature. These samples were designated as Hya-coated PEEK in the testing group. The cell studies were conducted using Hya-coated PEEK, uncoated PEEK, and cells only as control group.

2.2. Surface characteristics of the samples

2.2.1. Surface free energy (hydrophilicity test)

The wettability of a material was assessed using the "sessile drop technique" on four samples of Hya-coated and uncoated PEEK. The contact angle of two drops of 5 μL deionized water was measured. Images were captured utilizing ZEISS CCD microscope cameras and Labomed stereo microscopes. Photographs were taken 10 s after the liquid was released to document a uniform downward motion. ImageJ contact angle plugin was used to measure the angle.

2.2.2. Attenuated total reflectance - fourier transform infrared spectroscopy (ATR-FTIR)

FT-IR spectra (600–4000 cm − 1) of uncoated and Hya-coated PEEK samples in KBr pellets were recorded via a Nicolet 6700 FT-IR spectrometer using Omnic 8.0 software (ThermoFisher Scientific, Waltham, MA, USA). 64 scans with a spectral resolution of 2.0 cm − 1 were obtained. The spectra were 11-point smoothed, baseline corrected, and exported in ASCII format using Origin 6.0 (Microcal Origin, Northampton, MA, USA) graph preparation software. A second derivative technique was used to calculate the shoulder position.

2.2.3. Atomic force microscope (AFM)

The samples' roughness characteristics were investigated by AFM using a Veeco SPM (digital instrument) microscope and estimated for the scanned region (5 μm × 5 μm) using Gwiddyon software.

2.3. Cell culture

The National Center of Genetic Resources in Iran provided MG-63 cells (ATCC: C555) which were cultured in Dulbecco's Modified Eagle Medium (DMEM) (GIBCO ™ 41965039) with 10 % fetal bovine serum (FBS), streptomycin sulfate (100 mg/mL), and penicillin (100 U/mL). After incubation at 37 °C with 5 % CO_2, cells were examined for foreign bodies, contaminated medium, and nonviable cells. The cells were then incubated for 7 days to achieve the desired density, and the medium was changed every three days.

2.3.1. Cell viability (MTT assay)

The disks were placed in a 24-well plate, seeded with 5 × 104 MG-63 cells per well, and incubated for 7 and 21 days at 37 °C. 100 μl of MTT (MTT stock-diluted 1:10 in culture media) was applied to each well after a stock solution of 3-(4,5-dimethylthiazol-2-yl)-2,5-diphenyl-2H-tetrazolium bromide (MTT) was prepared. The plates were incubated for 3–4 h at 37 °C. The assay detects the change in color when MTT (yellow) is converted to formazan(purple) crystal, which can be used to determine the percentage of viable cell. Following incubation, the cells' supernatant was removed, and each well received 100 μl of dimethylsulfoxide (DMSO) for 15 min, which helped to dissolve the crystal. The disks were taken out of the wells following the DMSO solvent's solution. A spectrophotometer was used to measure the absorbance at a wavelength of 570 nm.The survival percentage of each treatment sample is determined as (treatment sample absorption / control sample absorption) × 100.

2.3.2. Cell proliferation (DAPI staining protocol)

Cells were seeded in 24-well plates and cultivated for 21 days at 37 °C and 5 % CO_2. After removing the media on day 21, they were rinsed with phosphate-buffer saline (PBS) and fixed with 4 % paraformaldehyde (Merck, Darmstadt, Germany) at 4 °C for 5 min. After washing with sterile distilled water, the samples were incubated in 1 μg/mL 4′,6-diamidino-2-phenylindole (DAPI) stain at 25 °C for 10 min. Excess dye was rinsed with sterile water. All samples were visually inspected using a fluorescent microscope (Olympus) at a magnification of × 400, using the OLYSIA Bio Report Soft Imaging System GmbH, Version: 3.2 (Build 670).

2.3.3. Alkaline phosphatase (ALP) activity

ALP production in osteoblast was measured using a commercial enzyme-linked Immunosorbent assay (ELISA) kit for human ALP (Zellbio GmbH, Germany) according to the manufacture instruction. Approximately 5 × 10^4 osteoblasts were cultured in 24-well plate for 7 and 21 days. Absorbance at 450 nm was measured in an ELISA plate reader (Zellbio GmbH, Germany).

2.3.4. Alizarin red staining

After 7 and 21 days, the cells were washed in PBS, fixed for 10 min at 4 °C in 4 % paraformaldehyde (Merck, Darmstadt, Germany), and stained for 10 min in PBS with 0.5 % Alizarin Red S. Bounded Alizarin Red was dissolved for 2 h at 37 °C using 10 % cetylpyridinium chloride-CPC in 10 mM Na2HPO4 (pH=7). Optical absorption was measured at

630 nm using a spectrophotometer and a microplate reader (Biotek Plate Reader, Winooski, VT, USA).

2.4. Statistical analysis

The data were analyzed using IBM SPSS Statistics for Windows 26.0, confirming normality and homogeneity through Shapiro-Wilk and Levene's tests, followed by one-way ANOVA and post hoc Tukey analysis, with a P-value of less than 0.05 indicating statistical significance.

3. Results

3.1. Hydrophilicity test

Fig. 1 shows the contact angle data. The uncoated PEEK sample exhibited the lowest wettability (94.5°) and the wettability of Hya-coated PEEK (22.9°) significantly increased after sandblasting and atmosphere-plasma treatment with low-pressure oxygen gas.

3.2. ATR-FTIR

Fig. 2 depicts the FTIR spectrum of Hya-coated PEEK, which is differentiated by several peaks representing the intrinsic functional groups of the component materials. PEEK shows aromatic C–H stretching at 2983.45 and 2921.74 cm^{-1}, confirming the existence of aromatic rings despite low intensity. The C=O ketone stretching at 1533.19 cm^{-1} may identify ketone groups in PEEK and carboxylic groups in Hya. Peaks at 1398.19 cm^{-1} and 1014.41 cm^{-1} indicate Ether C-O-C stretching in PEEK polymer chains and sugar moieties in Hya.

3.3. AFM

Fig. 3 shows the three-dimensional morphology of the Hya-coated and uncoated PEEK disks by AFM. The uncoated and Hya-PEEK surfaces exhibited different morphologies. Before coating, the average roughness (Ra) was 290.7 nm; after coating, it was 79.1 nm. After coating, the root mean square (RMS) values of the samples decreased from 337 nm to 100.3 nm. Comparison of the Hya- coated PEEK specimen with the uncoated surface revealed that the roughness of the former was reduced.

3.4. Cell viability (MTT protocol)

Table 1 shows results of cell viability, proliferation, ALP, and alizarin red staining. Fig. 5A shows the effect of the Hya on cell viability in the MTT assay. The viability of MG-63 cells increased in all the groups. The Hya-coated group showed increased cell viability at 7 and 21 days compared with the uncoated PEEK and control groups (P<0.001).

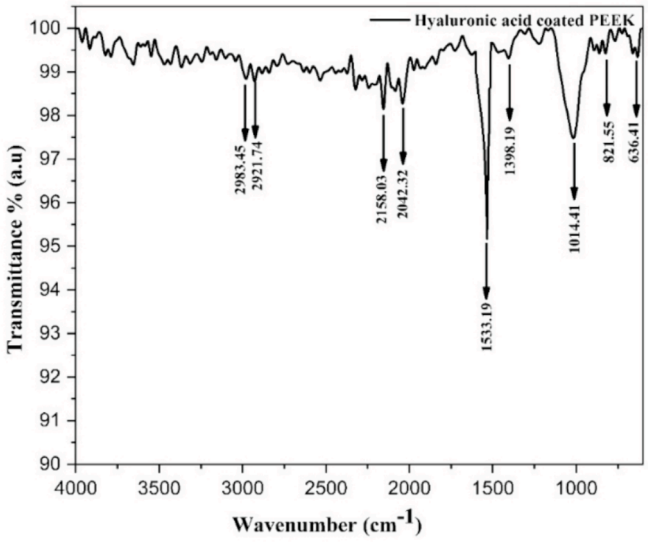

Fig. 2. FTIR spectrum of Hya-coated PEEK obtained in ATR mode.

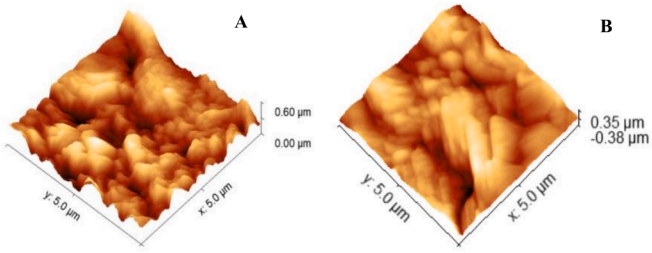

Fig. 3. AFM of the samples (a) uncoated PEEK disk;(b) Hya-coated PEEK.

Throughout the incubation period, the uncoated PEEK group showed considerably higher cell viability than the control group (P<0.02).

3.5. Cell proliferations (DAPI staining protocol)

Hya surface treatment increased MG-63 cell numbers and biocompatibility, which were statistically significant compared to the control cells (P<0.001) and cells adhered to uncoated PEEK (P <0.002). The growth of cells on uncoated PEEK was substantially greater than that of control cells by day 21 (P<0.001). Phalloidin/DAPI immunofluorescence labeling revealed the proliferation of cells on the Hya-coated and untreated PEEK surfaces (Fig. 4).

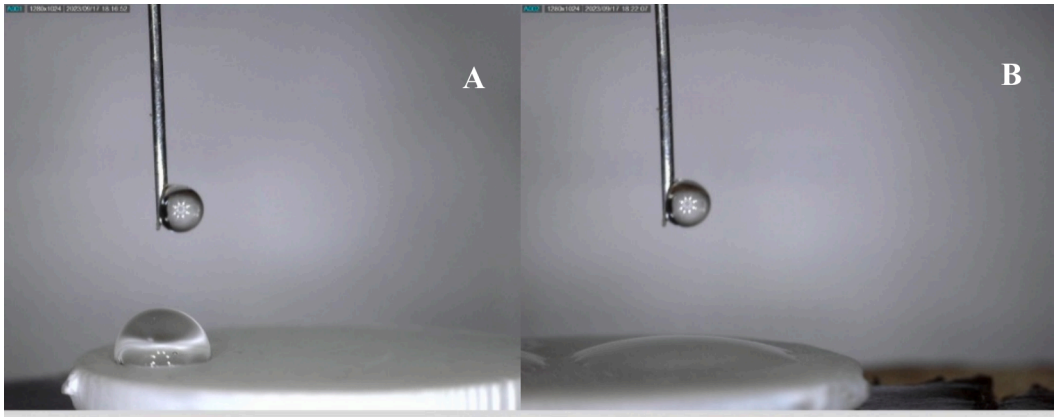

Fig. 1. Hydrophilicity test. (A) PEEK disk before Plasma surface treatment; (B). PEEK disk after plasma surface treatment.

Table 1
The biological analysis results of the different studied groups.

biological tests	Cells only (control)	Uncoated PEEK	Hya- coated PEEK
MTT assay			
Level 7 days			
Mean ± SD	0.98 ± 0.04	1.19 ± 0.06	1.48 ± 0.13
Median (Min. – Max.)	0.99 (0.92–1.04)	1.18 (1.12–1.27)	1.47 (1.29–170)
Level 21 days			
Mean ± SD	1.00 ± 0.07	1.26 ± 0.07	1.49 ± 0.09
Median (Min. – Max.)	1.00 (0.88–1.11)	1.23 (1.18–1.36)	1.48 (1.37–1.63)
DAPI staining assay			
Level 21 days			
Mean ± SD	38.33 ± 4.88	50.33 ± 2.58	60.50 ± 3.08
Median (Min. – Max.)	38.00 (32.00–46.00)	51.00 (46.00–53.00)	61.50 (58.00–73.00)
ALP activity			
Level 7 days			
Mean ± SD	0.16 ± 0.09	1.08 ±0.49	table5.55 ± 0.65
Median (Min. – Max.)	0.14 (0.07–0.30)	1.05 (0.29—0 1.75)	5.59 (4.81–6.35)
Level 21 days			
Mean ± SD	0.34 ± 0.18	2.59 ± 0.68	7.54 ± 0.64
Median (Min. – Max.)	0.29 (0.19–0.70)	2.60 (1.60–3.63)	7.66 (6.75–8.29)
Alizarin red staining			
Level 7 days			
Mean ± SD	0.99 ± 0.10	1.12 ± 0.17	1.81 ± 0.23
Median (Min. – Max.)	0.98 (0.90–1.14)	1.10 (0.88 – 1.36)	1.80 (1.57–2.18)
Level 21 days			
Mean ± SD	0.98 ± 0.05	1.14 ± 0.19	1.97 ± 0.20
Median (Min. – Max.)	1.00 (0.91–1.05)	1.12 (0.96 – 1.40)	1.95 (1.74–2.28)

PEEK: polyether ether ketone; MTT: 3-(4,5-dimethylthiazol-2-yl)-2,5-diphenyl-2H-tetrazolium bromide; DAPI: 4′,6-diamidino-2-phenylindole; ALP: alkaline phosphatase activity.

3.6. ALP activity

Fig. 5B shows the ALP activity of the MG-63 cells line on different substrates. On days 7 and 21, the cells cultured on Hya-coated PEEK disks showed significantly higher ALP activity than those cultured on untreated PEEK disks and control cells ($P < 0.001$). Cells grown on uncoated PEEK disks showed greater ALP activity than control cells ($P < 0.02$).

3.7. Alizarin red staining

Alizarin red staining at 7 and 21 days was used to quantify the sample mineralization potential (Fig. 5C). Cells grown on Hya-coated PEEK showed stronger extracellular matrix mineralization than the control and uncoated groups at both time points ($P < 0.001$). Hya-coated PEEK consistently outperformed the control and uncoated PEEK groups in terms of mineralization ($P < 0.05$).

4. Discussion

PEEK is biocompatible and chemically resistant, making it a feasible substitute for metallic alloys in orthopedic treatments (Lecocq et al., 2017). PEEK is used in dental implant infrastructures, abutments, and fixtures but lacks osteoconductivity and is bioinert. Bioactive coatings improve reliability of osseointegration. Few studies have used PEEK as a dental implant, suggesting there is insufficient evidence to show that it can replace titanium for dental implants, despite its promise.

The hydrophilicity test revealed increased hydrophilicity and significant changes in surface roughness after Hya coating, confirming the success of the coating process. Sandblasting and plasma surface treatment are commonly used in industrial procedures because of their cost-effectiveness and simplicity (Gravis et al., 2018). Oxygen plasma treatment changes fluorine-free polymers. Plasma activated reactive oxygen species exchange hydrogen atoms or break bonds on polymer surfaces, creating hydroxyl, epoxy, carbonyl, and carboxyl functional groups (Mozetič, 2020). These surface functional groups boost the polar surface energy and wettability, and increased wettability boosts the coating adherence to PEEK samples (Fukunaga et al., 2020). However, the exact mechanism underlying this relationship remains unknown. Hya coating reduced the surface roughness of the PEEK surfaces, similar to other bioactive and nanoparticle treatments (Liu et al., 2018). Biomaterial surface roughness's affects bacterial adherence and dispersion. Smoother surfaces prevent infections from adhering and growing (Wu et al., 2020).

After coating, AFM and ATR-FTIR showed Hya on the surface. The PEEK polymer chain reveals the presence of Hya sugar moieties through ether C-O-C stretching at 1398.19 cm^{-1} and 1014.41 cm^{-1}, and the C=O ketone stretching at 1533.19 cm-1 distinguishes ketone and carboxylic groups in Hya. The absence of the O–H stretching peak around 3400 $cm^{-}1$, attributed to hyaluronic acid's hydroxyl groups, suggests a chemical interaction between PEEK and hyaluronic acid. (Kwon et al., 2018; Pan et al., 2017).

These findings indicate that Hya and plasma oxygen boost cell growth and survival. This is crucial for the biological application of this modified polymer. Hya inhibited apoptosis and promoted cell survival. Cell viability on a substance requires cell adherence, making cell migration, diffusion, proliferation, and differentiation feasible. This enhances collagen production, wound healing, and tissue regeneration. Hya may be degraded by reactive oxygen and nitrogen species, and its surface energy, mechanical characteristics, wettability, and substrate roughness can affect cell adhesion (Cai et al., 2020).

Research has shown that Hya-coated PEEK enhances osteoblast viability, proliferation, ALP activity, and alizarin red staining, indicating improved cellular differentiation and mineralization. Polymeric materials have better hydrophobicity and lower surface energies than metallic and ceramic materials (Sundriyal et al., 2021). The greater

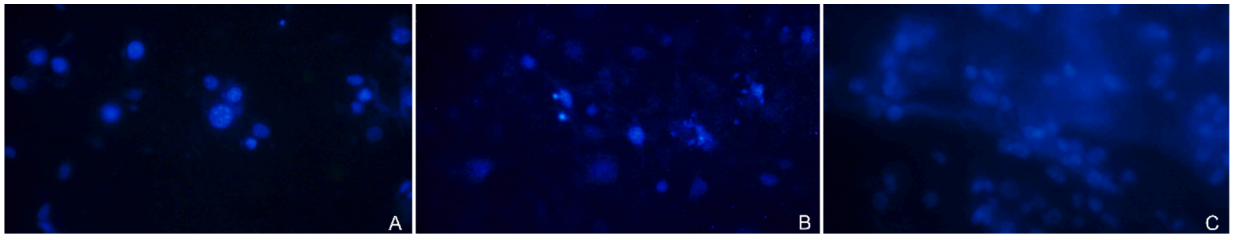

Fig. 4. Direct cell culture with DAPI (4′,6-diamidino-2-phenylindole)/phalloidin fluorescent imaging at 400 × after 21 days. (A) control; (B) uncoated PEEK; (C) Hya-coated PEEK. Blue color is from DAPI for visualizing cell nuclei. Scale bar 20 μm.

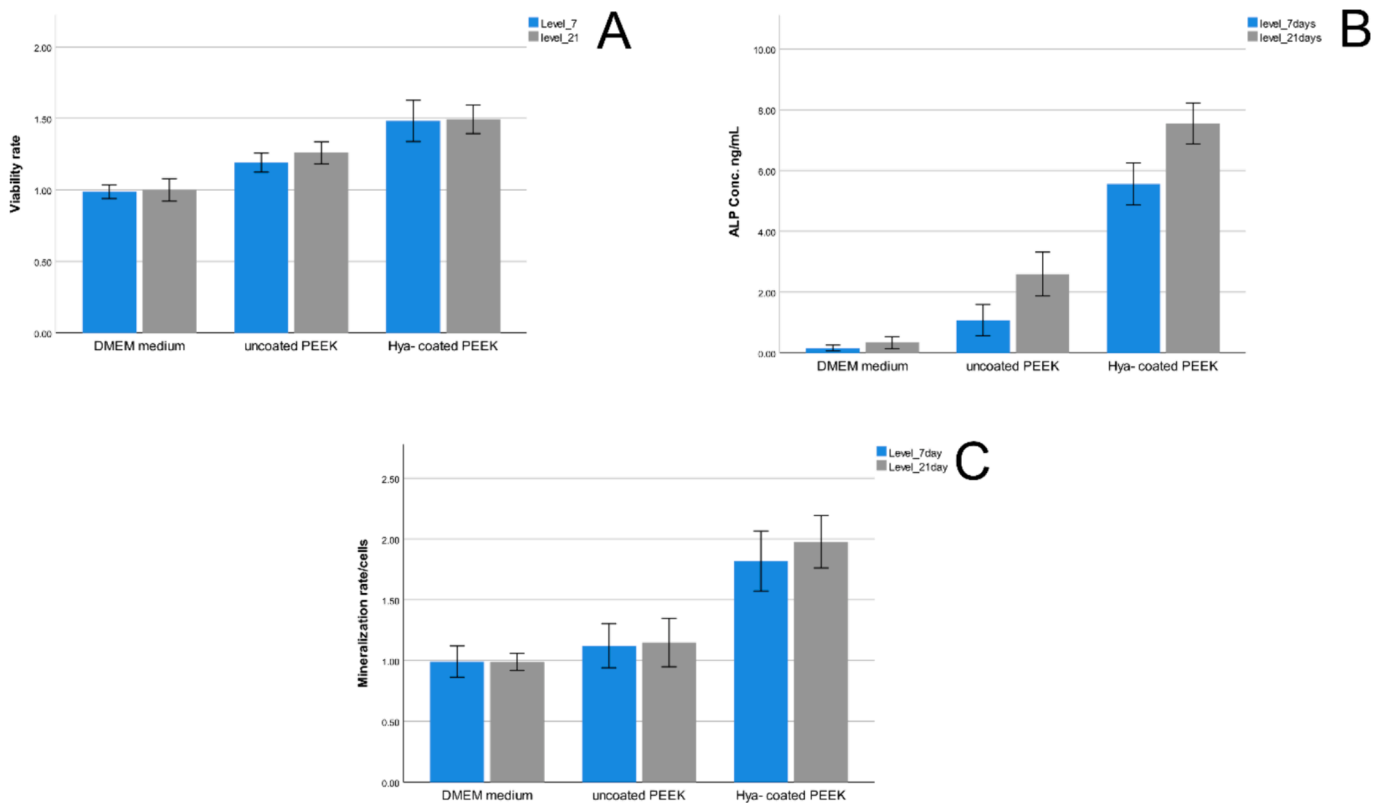

Fig. 5. A. The vitality rates of MG cell lines cultivated on several materials, including the control group, uncoated PEEK, and Hya coated PEEK, were compared. The rate was assessed at two distinct time points: 7 days (blue) and 21 days (grey). **B**. ALP activity for a MG-63 cell line grown on materials that have been treated. The absorbance at 450 nm is the measure of ALP activity. Each sample's ALP level was tested on days 7 (blue) and 21 (grey). The ALP activity of the Hya-coated PEEK was greater than that of the other two groups ($P<0.0001$), while the uncoated group's ALP activity rate was higher than that of the control group ($P<0.002$), indicating a substantial distinction between the groups. **C.** Extracellular matrix mineralization was measured using colorimetric methods, and the findings at 7 and 21 days (blue and grey, respectively) indicate that the Hya-coated PEEK group had a greater level than the control and uncoated PEEK groups ($P<0.001$).

polarity of PEEK helps cell membrane receptors (integrin) adhere via fibronectin and collagen (Peng et al., 2021). Surface roughness affect cell survival if it does not promote bacterial accumulation, surface poisoning, or cell death. Excessively rough surfaces can damage cells (Deligianni et al., 2001).

Bacterial contamination significantly contributes to implantation-associated infections, and strategies like biocide leaching, adhesion resistance, bacteria repulsion, and contact killing have been employed to minimize or avoid infection (Junter et al., 2016; Valverde et al., 2019). Hya, a hydrophilic substance with potential for bacteriostasis, has antibacterial properties due to its water-absorption capacity and chemical modifications, enhancing its electrostatic bacteria-killing properties (Junter et al., 2016; Lequeux et al., 2014).

The enzyme ALP regulates the metabolism of inorganic phosphate, which is essential for bone growth, by hydrolyzing phosphate esters, increasing the phosphate concentrations and promoting extracellular matrix mineralization (Yu et al., 2020). Calcium nodules, a characteristic of osteoblast populations, are typically identified using alizarin red staining during the latter phases of differentiation in osteoblast cultures (Kruger et al., 2011). Our results showed that the Hya-coated PEEK substrate significantly stimulates osteogenesis compared to the uncoated PEEK and the control, which is consistent with previous studies (D'Amora et al., 2019, 2018; Ronca et al., 2018).

Factors such as composition, shape, roughness, hydrophilicity, and functional groups of biomaterial surfaces significantly influence osteoblast differentiation, mineralization, osteoblast activities, and bone formation (Le Guéhennec et al., 2007). Rougher surfaces with higher hydrophilicity and surface energy may improve fibrin clot adhesion, cell proliferation, and osteogenic differentiation, possibly improving bone regeneration (Porrelli et al., 2021). The impact of biomaterial surface roughness and hydrophilicity on the growth potential of human osteosarcoma cell lines has been well-documented (Tseng et al., 2021).

Hya is widely used in medical fields such as tissue engineering because of its ability to promote bone growth, cell adhesion, and angiogenesis (Husseini et al., 2023a, 2023b; Liu et al., 2022). Carboxyl groups increase cell migration and proliferation by increasing water absorption and viscoelasticity (Agarwal et al., 2020). Hya inhibits BMP-2 antagonists and ERK phosphorylation to increase the osteogenic bioactivity of BMP-2 in MG63 cells. Its synergy with type I collagen may increase the inhibition of ERK phosphorylation in human mesenchymal stem cells and promote osteogenesis (Kawano et al., 2011).

Hya is broken down into fragments by hyaluronidases through hydrolysis of hexosaminidic β (1–4) linkages between N-acetyl-D-glucosamine and D-glucuronic acid. These fragments activate specific cell responses, including fibroblast proliferation and new vessel formation (Prosdocimi and Bevilacqua, 2012).

High-molecular weight Hya significantly impacts cellular activity, regulating migration, differentiation, and adhesion. It improves biocompatibility, viscosity, and residence duration (Li et al., 2020). In this study, high molecular weight Hya played a crucial role in cellular signaling and interactions with macromolecules.

Osseointegration requires at least 4 to 6 months. Histologically, Hya is retained for 8 weeks in implanted collagen matrices. Hya-coated titanium implants produced acceptable results (Yurttutan et al., 2023).

Hya interacts with various cell receptors, including CD44, RHAMM, TLRs, GHAP, ICAM-1, and LYVE-1(Itano, 2008). The primary Hya receptor is CD44, which affects cell division, proliferation (Johnson and Jackson, 2021), and bone metabolism (Bonifacio et al., 2023). RHAMM

regulates cell motility and growth factor response (Zhai et al., 2020). Hya may activate receptors, cytokines, and signaling complexes simultaneously, creating a complicated path that initiates cell differentiation and proliferation, and actives the appropriate genes (Zhao et al., 2016). Most studies have focused on the mesenchymal cell receptors CD44, RHAMM, and TLR4 (Lai et al., 2024). The interactions between Hya and these receptors can lead to cell differentiation and proliferation.

This study had some limitations. A cell line resembling osteoblasts was used in vitro, indicating the need for further in vivo studies to confirm these results. Further research is required to understand bacterial adherence and development on PEEK, particularly *peri*-implantitis, which is a significant issue affecting the long-term effectiveness of dental implants. However, these findings suggest that Hya-coated PEEK may be a viable substitute for dental implants.

5. Conclusion

This study revealed that Hya coating improves the surface biofunctionality and biomedical potential of PEEK by enhancing cell viability, proliferation, differentiation, and mineralization potential. These findings suggest the need for further research to enhance the osteogenic activity of PEEK materials, potentially expanding their applications in dental and orthopedic implantation.

Ethical statement

The study did not contain any human or animal subjects and did not involve ethical approval.

Declaration of competing interest

The authors declare that they have no known competing financial interests or personal relationships that could have appeared to influence the work reported in this paper.

Data availability

Data will be made available on request.

References

Abdulghafor, M.A., Mahmood, M.K., Tassery, H., Tardivo, D., Falguiere, A., Lan, R., 2024. Biomimetic coatings in implant dentistry: a quick update. J. Funct. Biomater. 15, 15. https://doi.org/10.3390/jfb15010015.

Agarwal, G., Agiwal, S., Srivastava, A., 2020. Hyaluronic acid containing scaffolds ameliorate stem cell function for tissue repair and regeneration. Int. J. Biol. Macromol. 165, 388–401.

Amengual-Peñafiel, L., Córdova, L.A., Constanza Jara-Sepúlveda, M., Brañes-Aroca, M., Marchesani-Carrasco, F., Cartes-Velásquez, R., 2021. Osteoimmunology drives dental implant osseointegration: A new paradigm for implant dentistry. Jpn. Dent. Sci. Rev. 57, 12–19. https://doi.org/10.1016/j.jdsr.2021.01.001.

Ananth, H., Kundapur, V., Mohammed, H.S., Anand, M., Amarnath, G.S., Mankar, S., 2015. A review on biomaterials in dental implantology. Int. J. Biomed. Sci. IJBS 11, 113.

Bonifacio, M.A., Cassano, A., Vincenti, A., Vinella, A., Dell'Olio, F., Favia, G., Mariggiò, M.A., 2023. In vitro evaluation of the effects of hyaluronic acid and an aminoacidic pool on human osteoblasts. Biomedicines 11, 751.

Bosshardt, D.D., Chappuis, V., Buser, D., 2017. Osseointegration of titanium, titanium alloy and zirconia dental implants: current knowledge and open questions. Periodontol. 2000 (73), 22–40. https://doi.org/10.1111/prd.12179.

Cai, S., Wu, C., Yang, W., Liang, W., Yu, H., Liu, L., 2020. Recent advance in surface modification for regulating cell adhesion and behaviors. Nanotechnol. Rev. 9, 971–989. https://doi.org/10.1515/ntrev-2020-0076.

Chatzopoulos, G.S., Wolff, L.F., 2023. Survival rate of implants performed at sites of previously failed implants and factors associated with failure: a retrospective investigation. J. Dent. Sci. https://doi.org/10.1016/j.jds.2023.10.012.

Chen, Z., Chen, Y., Ding, J., Yu, L., 2023. Blending strategy to modify PEEK-based orthopedic implants. Compos. Part B Eng. 250, 110427 https://doi.org/10.1016/j.compositesb.2022.110427.

D'Amora, U., Ronca, A., Raucci, M.G., Lin, H., Soriente, A., Fan, Y., Zhang, X., Ambrosio, L., 2018. Bioactive composites based on double network approach with tailored mechanical, physico-chemical, and biological features. J. Biomed. Mater. Res. A 106, 3079–3089. https://doi.org/10.1002/jbm.a.36498.

D'Amora, U., Ronca, A., Raucci, M.G., Dozio, S.M., Lin, H., Fan, Y., Zhang, X., Ambrosio, L., 2019. In situ sol-gel synthesis of hyaluronan derivatives bio-nanocomposite hydrogels. Regen. Biomater. 6, 249–258.

Deligianni, D.D., Katsala, N., Ladas, S., Sotiropoulou, D., Amedee, J., Missirlis, Y.F., 2001. Effect of surface roughness of the titanium alloy Ti–6Al–4V on human bone marrow cell response and on protein adsorption. Biomaterials 22, 1241–1251. https://doi.org/10.1016/S0142-9612(00)00274-X.

Fukunaga, Y., Longo, R.C., Ventzek, P.L., Lane, B., Ranjan, A., Hwang, G.S., Hartmann, G., Tsutsumi, T., Ishikawa, K., Kondo, H., 2020. Interaction of oxygen with polystyrene and polyethylene polymer films: A mechanistic study. J. Appl. Phys. 127.

George, R., Maiti, S., Ganapathy, D.M., 2023. Estimation of L-carnitine levels in diabetic completely edentulous patients for implant diagnosis: a cross-sectional study. Dent. Res. J. 20, 96.

Gravis, D., Poncin-Epaillard, F., Coulon, J., 2018. Role of adsorbed water on PEEK surfaces prior to – and after – atmospheric plasma activation. Plasma Process. Polym. 15, 1800007. https://doi.org/10.1002/ppap.201800007.

Husseini, B., Friedmann, A., Wak, R., Ghosn, N., Khoury, G., El Ghoul, T., Abboud, C.K., Younes, R., 2023a. Clinical and radiographic assessment of cross-linked hyaluronic acid addition in demineralized bovine bone based alveolar ridge preservation: A human randomized split-mouth pilot study. J. Stomatol. Oral Maxillofac. Surg. 124, 101426 https://doi.org/10.1016/j.jormas.2023.101426.

Husseini, B., Friedmann, A., Wak, R., Ghosn, N., Senni, K., Changotade, S., Khoury, G., Younes, R., 2023b. The "HAT-TRICK" technique: A modification of soft tissue grafting using volume stable collagen matrix and cross-linked hyaluronic acid. Part A: The pontic site. J. Stomatol Oral Maxillofac. Surg. 125, 101754 https://doi.org/10.1016/j.jormas.2023.101754.

Ismail, R., Hasan, R., 2021. Evaluation of Patient's Satisfaction with Implant Supported Prosthesis in Rizgary Hospital from 2015–2019. Sulaimani Dent. J. 8, 6. https://doi.org/10.17656/sdj.10140.

Itano, N., 2008. Simple primary structure, complex turnover regulation and multiple roles of hyaluronan. J. Biochem. (tokyo) 144, 131–137.

Johnson, L.A., Jackson, D.G., 2021. Hyaluronan and its receptors: key mediators of immune cell entry and trafficking in the lymphatic system. Cells 10, 2061.

Junter, G.-A., Thébault, P., Lebrun, L., 2016. Polysaccharide-based antibiofilm surfaces. Acta Biomater. 30, 13–25. https://doi.org/10.1016/j.actbio.2015.11.010.

Kannan, K.P., Gunasekaran, V., Sreenivasan, P., Sathishkumar, P., 2024. Recent updates and feasibility of nanodrugs in the prevention and eradication of dental biofilm and its associated pathogens—A review. J. Dent. 143, 104888 https://doi.org/10.1016/j.jdent.2024.104888.

Kawano, M., Ariyoshi, W., Iwanaga, K., Okinaga, T., Habu, M., Yoshioka, I., Tominaga, K., Nishihara, T., 2011. Mechanism involved in enhancement of osteoblast differentiation by hyaluronic acid. Biochem. Biophys. Res. Commun. 405, 575–580. https://doi.org/10.1016/j.bbrc.2011.01.071.

Krishnakumar, S., Senthilvelan, T., 2021. Polymer composites in dentistry and orthopedic applications-a review. Mater. Today Proc., International Mechanical Engineering Congress 2019 46, 9707–9713. DOI: 10.1016/j.matpr.2020.08.463.

Kruger, E.A., Im, D.D., Bischoff, D.S., Pereira, C.T., Huang, W., Rudkin, G.H., Yamaguchi, D.T., Miller, T.A., 2011. In vitro mineralization of human mesenchymal stem cells on three-dimensional type I collagen versus PLGA scaffolds: a comparative analysis. Plast. Reconstr. Surg. 127, 2301–2311.

Kwon, G., Kim, H., Gupta, K.C., Kang, I.-K., 2018. Enhanced Tissue Compatibility of Polyetheretherketone Disks by Dopamine-Mediated Protein Immobilization. Macromol. Res. 26, 128–138. https://doi.org/10.1007/s13233-018-6018-z.

Lai, Y., Lu, X., Liao, Y., Ouyang, P., Wang, H., Zhang, X., Huang, G., Qi, S., Li, Y., 2024. Crosstalk between glioblastoma and tumor microenvironment drives proneural–mesenchymal transition through ligand-receptor interactions. Genes Dis. 11, 874–889. https://doi.org/10.1016/j.gendis.2023.05.025.

Le Guéhennec, L., Soueidan, A., Layrolle, P., Amouriq, Y., 2007. Surface treatments of titanium dental implants for rapid osseointegration. Dent. Mater. 23, 844–854.

Lecocq, M., Bernard, C., Felix, M.S., Linares, J.-M., Chaves-Jacob, J., Decherchi, P., Dousset, E., 2017. Biocompatibility of four common orthopedic biomaterials following a high-salt diet: An in vivo study. Int. J. Mol. Sci. 18, 1489.

Lequeux, I., Ducasse, E., Jouenne, T., Thebault, P., 2014. Addition of antimicrobial properties to hyaluronic acid by grafting of antimicrobial peptide. Eur. Polym. J. 51, 182–190. https://doi.org/10.1016/j.eurpolymj.2013.11.012.

Li, C., Cao, Z., Li, W., Liu, R., Chen, Y., Song, Y., Liu, G., Song, Z., Liu, Z., Lu, C., Liu, Y., 2020. A review on the wide range applications of hyaluronic acid as a promising rejuvenating biomacromolecule in the treatments of bone related diseases. Int. J. Biol. Macromol. 165, 1264–1275. https://doi.org/10.1016/j.ijbiomac.2020.09.255.

Li, H., Huang, D., Ren, K., Ji, J., 2021. Inorganic-polymer composite coatings for biomedical devices. Smart Mater. Med. 2, 1–14. https://doi.org/10.1016/j.smaim.2020.10.002.

Liu, L., Jia, W., Zhou, Y., Zhou, H., Liu, M., Li, M., Zhang, X., Gu, G., Chen, Z., 2022. Hyaluronic acid oligosaccharide-collagen mineralized product and aligned nanofibers with enhanced vascularization properties in bone tissue engineering. Int. J. Biol. Macromol. 206, 277–287.

Liu, S., Zhu, Y., Gao, H., Ge, P., Ren, K., Gao, J., Cao, Y., Han, D., Zhang, J., 2018. One-step fabrication of functionalized poly(etheretherketone) surfaces with enhanced biocompatibility and osteogenic activity. Mater. Sci. Eng. C 88, 70–78. https://doi.org/10.1016/j.msec.2018.03.003.

Luo, Y., Tan, J., Zhou, Y., Guo, Y., Liao, X., He, L., Li, D., Li, X., Liu, Y., 2023. From crosslinking strategies to biomedical applications of hyaluronic acid-based hydrogels: A review. Int. J. Biol. Macromol. 231, 123308 https://doi.org/10.1016/j.ijbiomac.2023.123308.

Mahmood, M., Mahmood, B., 2023. Clinical, Physiological, and Psychological Evaluation of Implant-Related Full Mouth Rehabilitation. Sulaimani Dent. J. 10, 9. https://doi.org/10.17656/sdj.10167.

Mozetič, M., 2020. Plasma-Stimulated Super-Hydrophilic Surface Finish of Polymers. Polymers 12, 2498. https://doi.org/10.3390/polym12112498.

Pan, N.C., Pereira, H.C.B., Da Silva, M.D.L.C., Vasconcelos, A.F.D., Celligoi, M.A.P.C., 2017. Improvement Production of Hyaluronic Acid by Streptococcus zooepidemicus in Sugarcane Molasses. Appl. Biochem. Biotechnol. 182, 276–293. https://doi.org/10.1007/s12010-016-2326-y.

Peng, T.-Y., Shih, Y.-H., Hsia, S.-M., Wang, T.-H., Li, P.-J., Lin, D.-J., Sun, K.-T., Chiu, K.-C., Shieh, T.-M., 2021. In Vitro Assessment of the Cell Metabolic Activity, Cytotoxicity, Cell Attachment, and Inflammatory Reaction of Human Oral Fibroblasts on Polyetheretherketone (PEEK) Implant-Abutment. Polymers 13, 2995. https://doi.org/10.3390/polym13172995.

Porrelli, D., Mardirossian, M., Crapisi, N., Urban, M., Ulian, N.A., Bevilacqua, L., Turco, G., Maglione, M., 2021. Polyetheretherketone and titanium surface treatments to modify roughness and wettability–Improvement of bioactivity and antibacterial properties. J. Mater. Sci. Technol. 95, 213–224.

Prosdocimi, M., Bevilacqua, C., 2012. Exogenous hyaluronic acid and wound healing: an updated vision. Panminerva Med. 54, 129–135.

Reddy, K.U.K., Verma, P.C., Rathi, A., Saravanan, P., 2023. A comprehensive mechanical characterization of *as-printed* and saliva soaked 3D printed PEEK specimens for low-cost dental implant applications. Mater. Today Commun. 36, 106438 https://doi.org/10.1016/j.mtcomm.2023.106438.

Ronca, A., D'Amora, U., Raucci, M.G., Lin, H., Fan, Y., Zhang, X., Ambrosio, L., 2018. A combined approach of double network hydrogel and nanocomposites based on hyaluronic acid and poly (ethylene glycol) diacrylate blend. Materials 11, 2454.

Rupp, F., Liang, L., Geis-Gerstorfer, J., Scheideler, L., Hüttig, F., 2018. Surface characteristics of dental implants: A review. Dent. Mater. 34, 40–57.

Sacks, G., Shah, V., Yao, L., Yan, C., Shah, D., Limeta, L., DeStefano, V., 2024. Polyaryletherketones: Properties and applications in modern medicine. Biomed. Technol. 6, 75–89. https://doi.org/10.1016/j.bmt.2023.11.002.

Ślusarczyk, K., Flejszar, M., Spilarewicz, K., Wytrwal, M., Awsiuk, K., Wolski, K., Raczkowska, J., Janiszewska, N., Chmielarz, P., 2024. On the way to increase osseointegration potential: Sequential SI-ATRP as promising tool for PEEK-based implant nano-engineering. Eur. Polym. J. 210, 112953 https://doi.org/10.1016/j.eurpolymj.2024.112953.

Sundriyal, P., Sahu, M., Prakash, O., Bhattacharya, S., 2021. Long-term surface modification of PEEK polymer using plasma and PEG silane treatment. Surf. Interfaces 25, 101253. https://doi.org/10.1016/j.surfin.2021.101253.

Tseng, S.-J., Cheng, C.-H., Lee, T.-M., Lin, J.-C., 2021. Studies of osteoblast-like MG-63 cellular proliferation and differentiation with cyclic stretching cell culture system on biomimetic hydrophilic layers modified polydimethylsiloxane substrate. Biochem. Eng. J. 168, 107946.

Valverde, A., Pérez-Álvarez, L., Ruiz-Rubio, L., Pacha Olivenza, M.A., García Blanco, M. B., Díaz-Fuentes, M., Vilas-Vilela, J.L., 2019. Antibacterial hyaluronic acid/chitosan multilayers onto smooth and micropatterned titanium surfaces. Carbohydr. Polym. 207, 824–833. https://doi.org/10.1016/j.carbpol.2018.12.039.

Wang, S., Zhao, X., Hsu, Y., He, Y., Wang, F., Yang, F., Yan, F., Xia, D., Liu, Y., 2023. Surface modification of titanium implants with Mg-containing coatings to promote osseointegration. Acta Biomater. 169, 19–44. https://doi.org/10.1016/j.actbio.2023.07.048.

Wu, H., Liu, T., Xu, Z., Qian, J., Shen, X., Li, Y., Pan, Y., Wang, D., Zheng, K., Boccaccini, A.R., 2020. Enhanced bacteriostatic activity, osteogenesis and osseointegration of silicon nitride/polyetherketoneketone composites with femtosecond laser induced micro/nano structural surface. Appl. Mater. Today 18, 100523.

Yokoi, T., Kusumoto, Y., Abe, Y., Watanabe, H., Sanda, M., Hara, M., Matsumoto, T., Baba, K., 2023. Association between the treatment choice of implant-supported fixed partial dentures and oral health-related quality of life in patients with a shortened dental arch: A preliminary observational study. J. Dent. Sci. https://doi.org/10.1016/j.jds.2023.11.013.

Yu, W., Zheng, Y., Li, H., Lin, H., Chen, Z., Tian, Y., Chen, H., Zhang, P., Xu, X., Shen, Y., 2020. The Toll-like receptor ligand, CpG oligodeoxynucleotides, regulate proliferation and osteogenic differentiation of osteoblast. J. Orthop. Surg. 15, 327. https://doi.org/10.1186/s13018-020-01844-x.

Yurttutan, E., Dereci, Ö., Karagöz, M.A., 2023. Biomechanical and Histologic Evaluation of Osseointegration of Titanium Dental Implants Modified by Various Combinations of Sandblasting, Acid-Etching, Hydroxyapatite, and Hyaluronic Acid Coating Techniques. Int. J. Oral Maxillofac. Implants 38.

Zhai, P., Peng, X., Li, B., Liu, Y., Sun, H., Li, X., 2020. The application of hyaluronic acid in bone regeneration. Int. J. Biol. Macromol. 151, 1224–1239.

Zhao, N., Wang, X., Qin, L., Zhai, M., Yuan, J., Chen, J., Li, D., 2016. Effect of hyaluronic acid in bone formation and its applications in dentistry. J. Biomed. Mater. Res. A 104, 1560–1569. https://doi.org/10.1002/jbm.a.35681.

Zheng, Z., Liu, P., Zhang, X., Jingguo xin, Yongjie wang, Zou, X., Mei, X., Zhang, Shuling, Zhang, Shaokun, 2022. Strategies to improve bioactive and antibacterial properties of polyetheretherketone (PEEK) for use as orthopedic implants. Mater. Today Bio 16, 100402. DOI: 10.1016/j.mtbio.2022.100402.

Zhou, G., Wang, F., Lin, G., Tang, B., Li, X., Ding, X., Wang, W., Zhang, J., Shi, Y., 2023. Novel coatings for the continuous repair of human bone defects. Colloids Surf. B Biointerf. 222, 113127 https://doi.org/10.1016/j.colsurfb.2023.113127.